Effects of Hydrophobic Chain Length on the Characteristics of the Micelles of Octaoxyethylene Tetradecyl $C_{14}E_8$, Hexadecyl $C_{16}E_8$, and Octadecyl $C_{18}E_8$ Ethers

Naoko Hamada and Yoshiyuki Einaga*

Department of Chemistry, Nara Women's University, Nara 630-8506, Japan

Received: November 18, 2004; In Final Form: February 12, 2005

Size, shape, and flexibility of micelles of octaoxyethylene tetradecyl $C_{14}E_8$, hexadecyl $C_{16}E_8$, and octadecyl $C_{18}E_8$ ethers in dilute aqueous solutions were determined at finite surfactant concentrations c by static light scattering (SLS) and dynamic light scattering experiments at several temperatures T below the critical points. The SLS results were successfully analyzed with the aid of the thermodynamic theory formulated with wormlike spherocylinder model for SLS of micelle solutions. The analysis yielded the molar mass M_w of the micelles as a function of c and the cross-sectional diameter d. The hydrodynamic radius R_H and the radius of gyration $\langle S^2\rangle^{1/2}$ of the micelles as functions of M_w were found to be also well-described by the corresponding theories for the wormlike spherocylinder or wormlike chain models. The results of the stiffness parameter λ^{-1} have revealed that the micelles are far from rigid rods but rather stiff compared with typical flexible polymers and they grow in size with increasing T to greater length for longer hydrophobic chains, i.e., alkyl groups of the surfactants. As the alkyl group becomes longer, the d value increased, while the spacings s between adjacent hexaoxyethylene chains on the micellar surface were found to remain substantially constant.

Introduction

Nonionic surfactants polyoxyethylene monoalkyl ethers C_iE_j form micelles of various shapes such as sphere, threadlike, and so on in dilute aqueous solutions. Here, i and j denote the number of carbon atoms in the alkyl group and that of repeating units in the oxyethylene group, respectively. The micelles are known to grow in size with increasing surfactant concentration and increasing temperature, in particular when approaching the lower consolute phase boundary.

If the micelles are long enough, then they assume polymerlike or wormlike shape, and then their solution properties become analogous to those of polymer solutions. Hitherto, polymerlike micelles, with certain similarities to real polymers have been, thus, characterized with the use of experimental techniques employed in the polymer solution studies, such as static (SLS) and dynamic light scattering (DLS),[1−6,9] small-angle neutron scattering (SANS),[10−12] viscometry,[12,13] pulsed-field gradient NMR,[2−5] and so forth. These studies afford characteristics of given micelles, including their shape, cross-sectional diameter, size, and size distribution. However, the micelles possess an essential difference from polymers in that the micellar size or length is not chemically fixed but rather fluctuates around an equilibrium value. Moreover, the micellar size and its distribution, in general, depend on surfactant concentration, temperature, intermicellar thermodynamic interactions, and other factors. It is formidably difficult to achieve separate evaluation of the micellar growth and the enhancement of the intermicellar interactions as functions of surfactant concentration. Therefore, interpretations of the observed results especially from the SLS and DLS experiments are highly challenging.

In the previous paper,[14] we have studied $C_{12}E_6$ and $C_{14}E_6$ micelles in dilute aqueous solutions by SLS and DLS measurements. The SLS data have been analyzed by using the thermodynamic theory[15,16] of light scattering for micellar solutions to yield the molar mass M_w of the micelle as a function of surfactant concentration. The results of the hydrodynamic radius R_H and mean-square radius of gyration $\langle S^2\rangle$ as functions of M_w have been found to be well-described by the corresponding theory[17−20] with the wormlike spherocylinder or chain model, providing the information of the micellar size, structure, and intrinsic flexibility.

In this work, we have applied the same method to micelles of octaoxyethylene tetradecyl $C_{14}E_8$, hexadecyl $C_{16}E_8$, and octadecyl $C_{18}E_8$ ethers and examined effects of the hydrophobic chain length of the surfactant molecules on the micellar characteristics.

Experimental Section

Materials. High-purity $C_{14}E_8$, $C_{16}E_8$, and $C_{18}E_8$ samples were purchased from Nikko Chemicals Co. Ltd. and used without further purification. The solvent water used was high-purity (ultrapure) water prepared with the Simpli Lab water purification system from Millipore Co.

Phase Diagram. Cloud-point temperatures of given test solutions were visually determined as the temperatures at which turbidity of the solutions became detectable when the temperature was gradually raised.

Static Light Scattering. SLS measurements were performed to obtain the weight-average molar mass M_w of the $C_{14}E_8$, $C_{16}E_8$, and $C_{18}E_8$ micelles. The scattering intensities were measured for each solution and for the solvent water at scattering angles θ ranging from 30° to 150° and at temperatures T ranging from 40.0 to 65.0 °C for $C_{14}E_8$ solutions, from 25.0 to 50.0 °C for $C_{16}E_8$ solutions, and from 30.0 to 50.0 °C for $C_{18}E_8$ solutions. The ratio $Kc/\Delta R_\theta$ was obtained for each solution as a function of θ and extrapolated to the zero-scattering angle to evaluate $Kc/\Delta R_0$. Here, c is the surfactant mass concentration,

* Author to whom correspondence should be addressed. E-mail: einaga@cc.nara-wu.ac.jp.

10.1021/jp044747d CCC: $30.25
Published on Web 03/17/2005

ΔR_θ is the excess Rayleigh ratio, and K is the optical constant defined as

$$K = \frac{4\pi^2 n^2 (\partial n/\partial c)_{T,p}{}^2}{N_A \lambda_0{}^4} \quad (1)$$

with N_A being Avogadro's number, λ_0 the wavelength of the incident light in a vacuum, n the refractive index of the solution, $(\partial n/\partial c)_{T,p}$ the refractive index increment, T the absolute temperature and p the pressure. The plot of $Kc/\Delta R_\theta$ versus $\sin^2(\theta/2)$ affords a good straight line for all of the micelle solutions studied. For $C_{18}E_8$ solutions, the apparent mean-square radius of gyration of the micelles was determined from the slope of the straight line as described below. For the other micelle solutions, $Kc/\Delta R_\theta$ was almost independent of θ.

The apparatus used is an ALV DLS/SLS-5000/E light-scattering photogoniometer and correlator system with vertically polarized incident light of 632.8 nm wavelength from a Uniphase Model 1145P He−Ne gas laser. For calibration of the apparatus, the intensity of light scattered from pure benzene was measured at 25.0 °C at a scattering angle of 90°, where the Rayleigh ratio $R_{UV}(90°)$ of pure benzene for unpolarized scattered light with polarized incident light at a wavelength of 632.8 nm was taken as 11.84×10^{-6} cm^{-1}.[21,22]

The micellar solutions were prepared by dissolving an appropriate amount of the surfactant in water. Complete mixing and micelle formation were achieved by stirring using a magnetic stirrer at least for 1 day. The solutions thus prepared were optically purified by filtration through a membrane of 0.20 μm pore size and transferred into optically clean NMR tubes 10 mm in diameter, which were used as scatterring cells. The weight concentrations w of test solutions were determined gravimetrically and converted to mass concentrations c by the use of the densities ρ of the solutions given below.

The refractive index increment $(\partial n/\partial c)_{T,p}$ was measured at 30.0, 40.0, and 50.0 °C and at 632.8 nm with a Union Giken R601 differential refractometer. The results were 0.1362 cm^3/g for $C_{14}E_8$ solutions, 0.1360 cm^3/g for $C_{18}E_8$ solutions, irrespective of temperature, and $0.1365-1.506 \times 10^{-4}$ $(T - 273.15)$ cm^3/g for $C_{16}E_8$ solutions.

Dynamic Light Scattering. DLS measurements were carried out to determine the translational diffusion coefficient D for the micelles in water at various temperatures in the one phase (L_1 phase) region below or between the phase separation boundaries shown below by the use of the same apparatus and light source as used in the SLS studies described above. The normalized autocorrelation function $g^{(2)}(t)$ of scattered light intensity $I(t)$, i.e.,

$$g^{(2)}(t) = \frac{\langle I(0)I(t)\rangle}{\langle I(0)\rangle^2} \quad (2)$$

was measured at scattering angles θ ranging from 30° to 150°.

All of the test solutions studied are the same as those used in the SLS studies. From the data for $g^{(2)}(t)$, we determined D by the equation

$$(^1/_2)\ln[g^{(2)}(t) - 1] = (^1/_2)\ln f - K_1 t + \cdots \quad (3)$$

$$D = \lim_{q\to 0} K_1/q^2 \quad (4)$$

Here, f is the coherent factor fixed by the optical system, K_1 is the first cumulant, and q is the magnitude of the scattering vector defined as

$$q = \frac{4\pi n}{\lambda_0} \sin(\theta/2) \quad (5)$$

It should be noted that the D values should be regarded as the z-average, since the micelles observed may have distribution in size.

Density. The solution density ρ required for the calculation of c was measured at 30.0, 40.0, and 50.0 °C with a pycnometer of the Lipkin−Davison type. The results (in g/cm^3) are summarized as:

for $C_{14}E_8$ solutions

$$\rho^{-1} = 0.9966 + 3.83 \times 10^{-4}(T - 273.15) - 3.93 \times 10^{-4} w \quad (6)$$

for $C_{16}E_8$ solutions

$$\rho^{-1} = 0.9929 + 3.94 \times 10^{-4}(T - 273.15) + [-3.96 \times 10^{-4} + 7.21 \times 10^{-6}(T - 273.15)]w \quad (7)$$

and for $C_{18}E_8$ solutions

$$\rho^{-1} = 0.9927 + 3.83 \times 10^{-4}(T - 273.15) + [-3.98 \times 10^{-4} + 1.10 \times 10^{-5}(T - 273.15)]w \quad (8)$$

These results yield the partial specific volume v (in cm^3/g) of the micelles as:

for $C_{14}E_8$ micelles

$$v = 0.9962 + 3.83 \times 10^{-4}(T - 273.15) \quad (9)$$

for $C_{16}E_8$ micelles

$$v = 0.9925 + 4.01 \times 10^{-4}(T - 273.15) \quad (10)$$

and for $C_{18}E_8$ micelles

$$v = 0.9923 + 3.94 \times 10^{-4}(T - 273.15) \quad (11)$$

Results

Phase Behavior. The phase diagrams of the $C_{14}E_8$ + water (unfilled circles), $C_{16}E_8$ + water (half-filled circles), and $C_{18}E_8$ + water (filled circles) systems are depicted in Figure 1. The cloud-point curves for the $C_{14}E_8$ + water and $C_{16}E_8$ + water systems represent only lower critical solution temperature (LCST)-type phase separation boundaries above which the solutions phase separate into two phases. However, the $C_{18}E_8$ + water system has two phase separation regions of the LCST and upper critical solution temperature (UCST) types. It is seen that the LCST-type phase boundaries shift to lower temperatures in the order of the $C_{14}E_8$, $C_{16}E_8$, and $C_{18}E_8$ micelle solutions. This phase behavior resembles the observations of polymer solutions, in which the critical temperature T_c is shifted to lower values with increasing polymer molecular weight, when the phase diagram of the LCST type is observed. Thus, the observations in Figure 1 suggest that the micellar size becomes larger as the alkyl chain of the surfactants becomes longer.

Static Light Scattering. In Figure 2, parts a−c, $Kc/\Delta R_0$ is plotted against c examined at various temperatures for all the solutions of the $C_{14}E_8$, $C_{16}E_8$, and $C_{18}E_8$ micelles, respectively. The data points at fixed T follow a curve convex downward whose curvature becomes less significant as T is increased, although they are rather scattered in some cases. We note that the errors in the present measurements are in general on the order of a few percent, but they sometimes become appreciable,

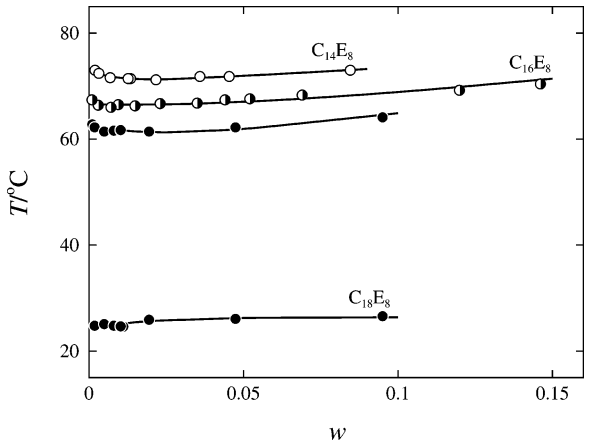

Figure 1. Phase diagrams of the $C_{14}E_8$ + water (unfilled circles), $C_{16}E_8$ + water (half-filled circles), and $C_{18}E_8$ + water (filled circles) systems.

especially at low temperatures and concentrations where the scattering intensities are rather weak. The $Kc/\Delta R_0$ value at fixed c decreases with increasing T. The $Kc/\Delta R_0$ value becomes smaller as the alkyl chain length of surfactant becomes larger, when compared at the same T and c.

Dynamic Light Scattering. Figure 3, parts a−c, illustrates the plots of D against c determined from the $g^{(2)}(t)$ data by the cumulant method with eqs 3 and 4 for the $C_{14}E_8$, $C_{16}E_8$, and $C_{18}E_8$ micelles at various temperatures, respectively. It is found that the D value becomes smaller as T is lowered, for any case of the micelle solutions, although the data points at low temperatures and concentrations are scattered due to the weakness in the intensity of the scattered light. The D value at fixed T and c decreases in the order of the $C_{14}E_8$, $C_{16}E_8$, and $C_{18}E_8$ micelles.

Discussion

Analysis of SLS Results. As mentioned in the Introduction, we have analyzed the present SLS data by employing a light-scattering theory for micellar solutions formulated by Sato,[15] with a wormlike spherocylinder model for polymerlike micelles, to determine the M_w values of the micelles at finite concentrations c. The model consists of a wormlike cylinder of contour length $L - d$ with cross-sectional diameter d and two hemispheres of diameter d that cap both ends of the cylinder. Stiffness of the wormlike cylinder is represented by the stiffness parameter λ^{-1}. It may represent a variety of shapes of the polymerlike micelles, including a sphere, rigid rod, flexible- and/or random-coil rod (or cylinder). The theoretical result of $Kc/\Delta R_0$ reads

$$\frac{Kc}{\Delta R_0} = \frac{1}{M_w(c)} + 2A(c)c \qquad (12)$$

where $M_w(c)$ is the weight-average molar mass of the micelles and $A(c)$ is the apparent second virial coefficient in a sense that it is comprised of the second, third, and the higher virial coefficient terms. Both are functions of c, containing three parameters d, free-energy parameter g_2, and strength $\hat{\epsilon}$ of the attractive interaction between spherocylinders. In these, g_2 represents the difference in Gibbs free energy between surfactant molecules located in the end-capped portion to those in the central cylindrical portion in the micelle. The parameter $\hat{\epsilon}$ is the depth of the attractive potential between cylindrical micelles. It should be noted that the micellar size, i.e., the aggregation number N of the surfactant molecules in the micelle, and its distribution are governed not only by multiple equilibria among the micelles with various N but also by the intermicellar interactions to some extent.[25] The parameters g_2 and $\hat{\epsilon}$ play dominant roles in the former and in the latter, respectively. We refer the readers to the expressions for the functions $M_w(c)$ and $A(c)$ from the original papers[15,16] and our previous paper,[14] since they are fairly involved.

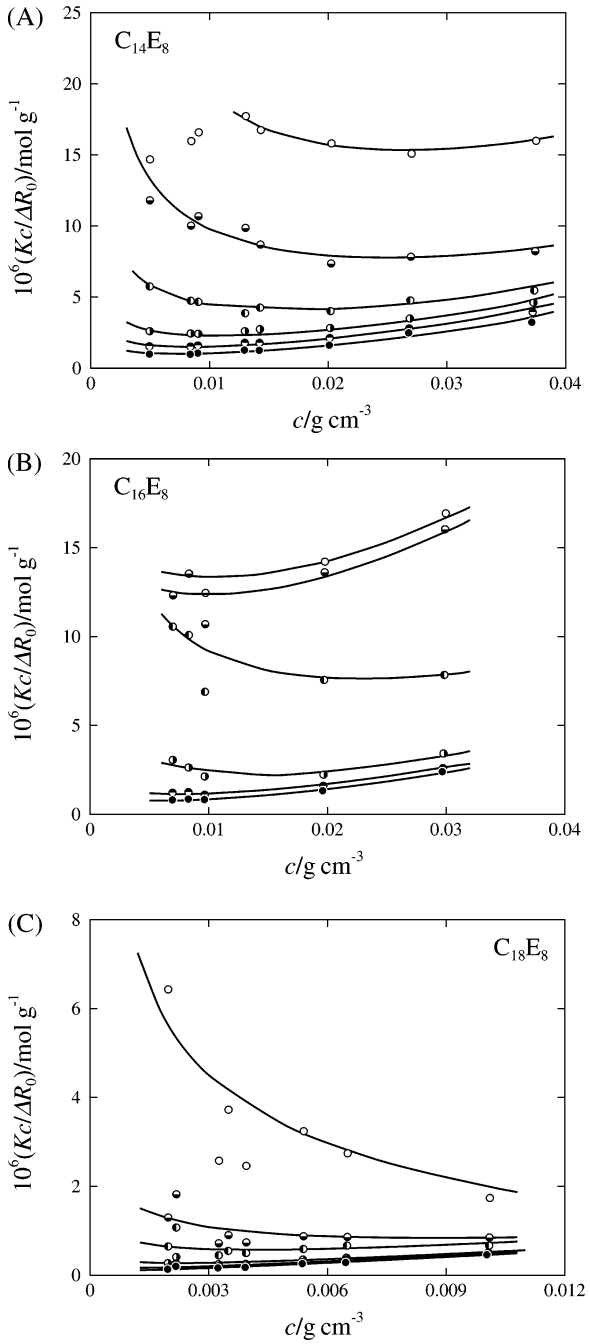

Figure 2. (a) Plots of $Kc/\Delta R_0$ versus c for the $C_{14}E_8$ solutions at various T. Temperatures T are 40.0, 45.0, 50.0, 55.0, 60.0, and 65.0 °C from top to bottom, respectively. (b) Plots of $Kc/\Delta R_0$ versus c for the $C_{16}E_8$ solutions at various T. Temperatures T are 25.0, 30.0, 35.0, 40.0, 45.0, and 50.0 °C from top to bottom, respectively. (c) Plots of $Kc/\Delta R_0$ versus c for the $C_{18}E_8$ solutions at various T. Temperatures T are 30.0, 33.0, 35.0, 40.0, 45.0, and 50.0 °C from top to bottom, respectively.

Figure 4, parts a−c, demonstrates the results of curve fitting of the theoretical calculations to the experimental values of $Kc/\Delta R_0$ for the $C_{14}E_8$, $C_{16}E_8$, and $C_{18}E_8$ micelle solutions, respectively. Here, the solid curves represent the best-fit theoretical values calculated by eq 12 by choosing the proper values of d,

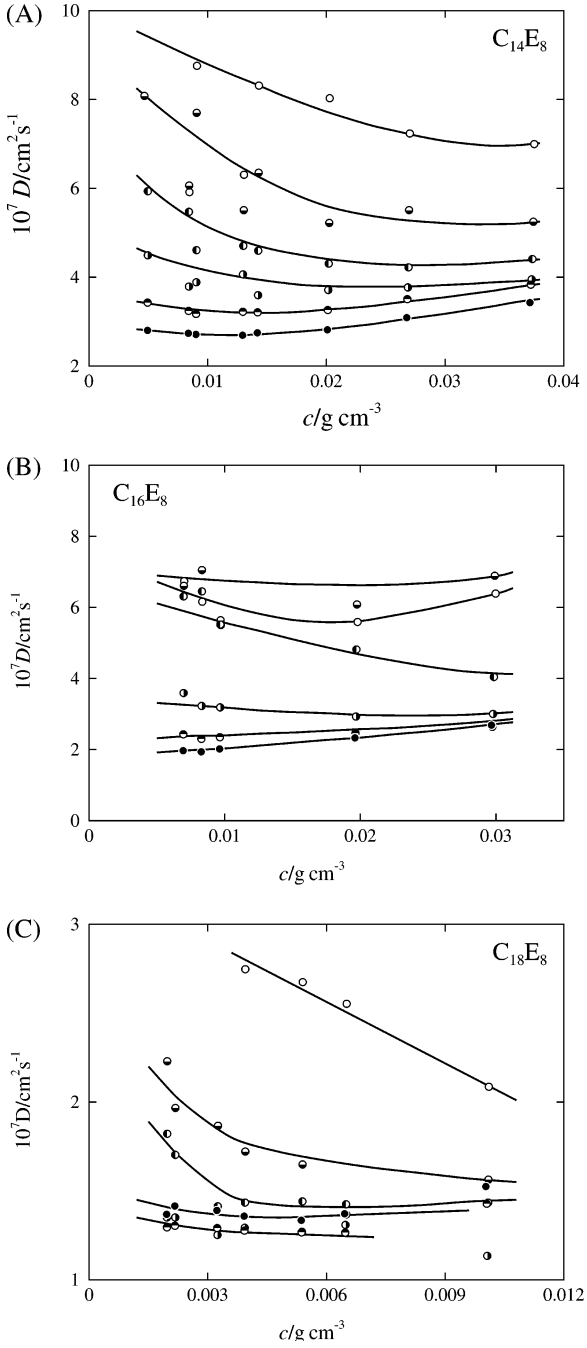

Figure 3. (a) Plots of D versus c for the $C_{14}E_8$ solutions at various T. Symbols have the same meaning as those in Figure 2a. (b) Plots of D versus c for the $C_{16}E_8$ solutions at various T. Symbols have the same meaning as those in Figure 2b. (c) Plots of D versus c for the $C_{18}E_8$ solutions at various T. Symbols have the same meaning as those in Figure 2c.

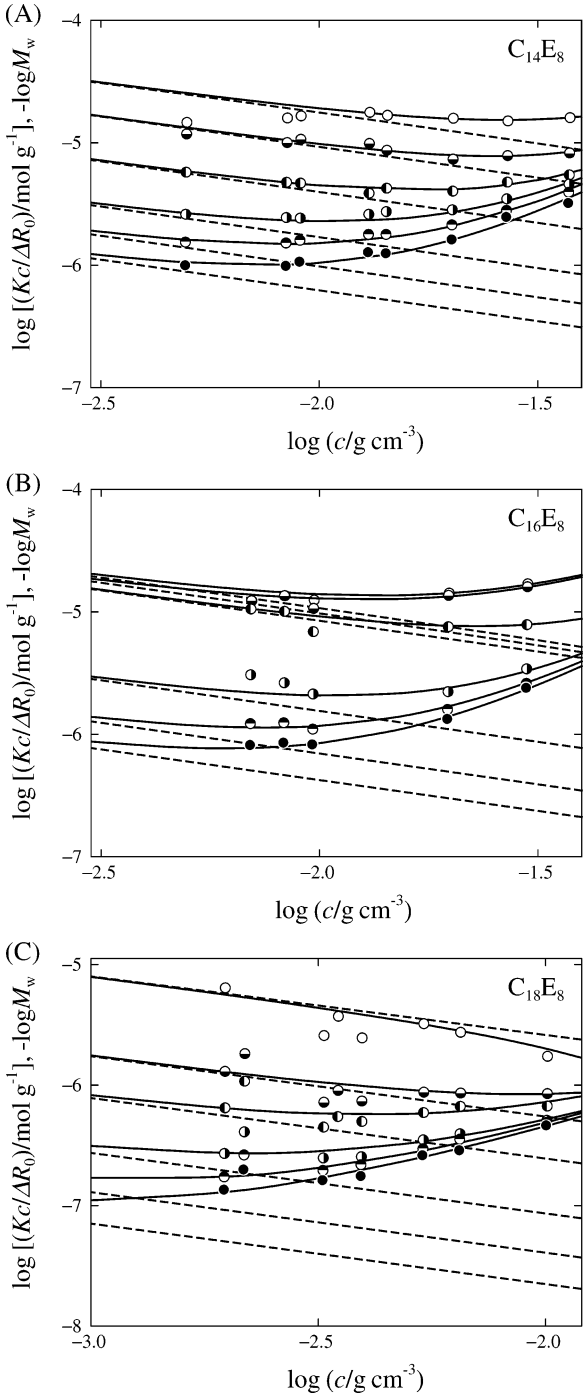

Figure 4. (a) The results of the curve fitting for the plots of $Kc/\Delta R_0$ versus c for the $C_{14}E_8$ solutions at various T. Symbols have the same meaning as those in Figure 2a. The solid and dashed curves represent $Kc/\Delta R_0$ and $1/M_w(c)$, respectively. Temperatures T are 40.0, 45.0, 50.0, 55.0, 60.0, and 65.0 °C from top to bottom, respectively. (b) The results of the curve fitting for the plots of $Kc/\Delta R_0$ versus c for the $C_{16}E_8$ solutions at various T. Symbols have the same meaning as those in Figure 2b. The solid and dashed curves represent $Kc/\Delta R_0$ and $1/M_w(c)$, respectively. Temperatures T are 25.0, 30.0, 35.0, 40.0, 45.0, and 50.0 °C from top to bottom, respectively. (c) The results of the curve fitting for the plots of $Kc/\Delta R_0$ versus c for the $C_{18}E_8$ solutions at various T. Symbols have the same meaning as those in Figure 2c. The solid and dashed curves represent $Kc/\Delta R_0$ and $1/M_w(c)$, respectively. Temperatures T are 30.0, 33.0, 35.0, 40.0, 45.0, and 50.0 °C from top to bottom, respectively.

g_2, and $\hat{\epsilon}$. It is seen that the solid curves are in good coincidence with the respective data points at given temperatures. The good agreement between the calculated and observed results implies that the $C_{14}E_8$, $C_{16}E_8$, and $C_{18}E_8$ micelles in dilute aqueous solutions are represented by the wormlike spherocylinder model. From the curve fitting, we have determined the M_w values of each micelle as a function of c. The dashed lines represent the values of $1/M_w(c)$ at respective temperatures. For all of the micelles at any fixed T, they have a slope of -0.5, showing that M_w increases with c following a relation $M_w \propto c^{1/2}$ in the range of c examined, as in the case of the previous findings for the $C_{12}E_6$ and $C_{14}E_6$ micelles.[14] These results are in good correspondence with simple theoretical predictions derived from the thermodynamic treatments of multiple equilibria among micelles of various aggregation numbers.[15,23,24,25] The solid and dashed curves coincide with each other at small c, and the

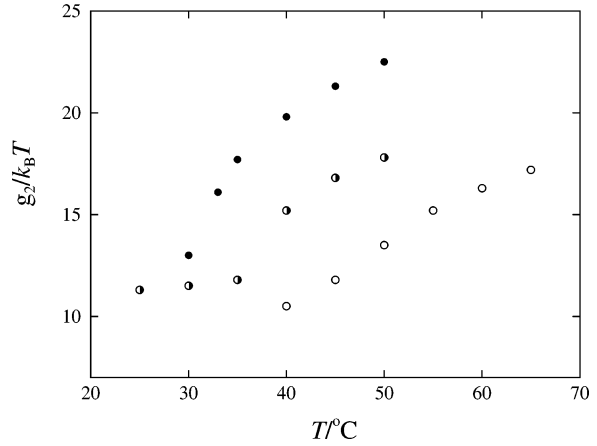

Figure 5. Temperature dependence of g_2 for the $C_{14}E_8$ + water (unfilled circles), $C_{16}E_8$ + water (half-filled circles), and $C_{18}E_8$ + water (filled circles) systems.

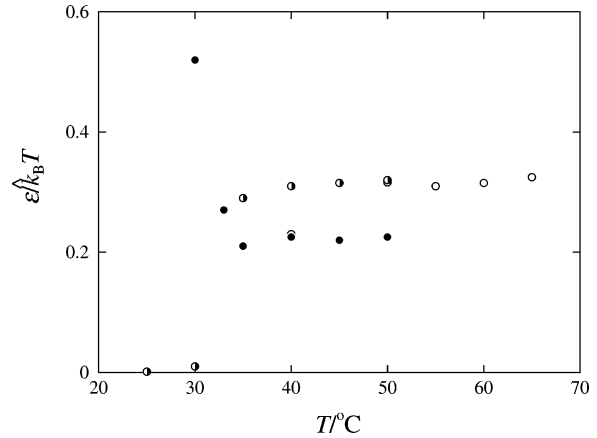

Figure 6. Temperature dependence of $\hat{\epsilon}$ for the $C_{14}E_8$ + water (unfilled circles), $C_{16}E_8$ + water (half-filled circles), and $C_{18}E_8$ + water (filled circles) systems.

difference between them steadily increases with increasing c. The results indicate that contributions of the virial coefficient terms, which is the second term of the right-hand side of eq 12, to $Kc/\Delta R_0$ are negligible at small c but progressively increase with increasing c as expected.

The d value chosen in the curve-fitting procedure is 2.3 ± 0.2 nm for $C_{14}E_8$ micelles, 2.4 ± 0.2 nm for $C_{16}E_8$ micelles, and 3.2 ± 0.5 nm for $C_{18}E_8$ micelles, at any T examined. Thus, the d value increases with increasing alkyl chain length of the surfactant. It should be mentioned that the last value for the $C_{18}E_8$ micelles might be somewhat errorneous, since the light-scattering results were limitted to the range of small c. The values of g_2 and $\hat{\epsilon}$ determined are plotted against T in Figures 5 and 6, respectively. It is found that when compared at fixed T, the g_2 value above 30.0 °C is larger for the C_iE_8 micelles with larger i. For each micelle, g_2 is an increasing function of T. However, $\hat{\epsilon}$ does not show clear systematic dependence on the surfactant species, but the data points are rather scattered in the narrow range of approximately 0.2−0.35 except for those at low T. These results for g_2 and $\hat{\epsilon}$ may reflect the fact that the alkyl group of the surfactant molecules becomes longer in the order of $C_{14}E_8$, $C_{16}E_8$, and $C_{18}E_8$, but the length of oxyethylene group is the same for all of the surfactants. Thus, attractive (hydrophobic) interactions among C_iE_8 molecules are considered to become stronger with increasing i.

Molar Mass Dependence of Radius of Gyration. From the slope of the $Kc/\Delta R_\theta$ versus $\sin^2(\theta/2)$ plot, we have determined the apparent mean-square radius of gyration $\langle S^2\rangle_{app}$ for the $C_{18}E_8$ micelles on the basis of the fundamental light-scattering equation

$$\frac{Kc}{\Delta R_\theta} = \frac{1}{M_w(c)}\left(1 + \frac{1}{3}\langle S^2\rangle q^2\right) + 2A_2c + \cdots \qquad (13)$$

at finite concentrations by using the $M_w(c)$ values determined as described above. Here, A_2 is the second virial coefficient, and $\langle S^2\rangle$ is denoted by $\langle S^2\rangle_{app}$, since it is possibly affected by intermicellar interactions. Here, we note that $\langle S^2\rangle_{app}$ was not evaluated for the $C_{14}E_8$ and $C_{16}E_8$ micelles, because angular dependence of $Kc/\Delta R_\theta$ for them was negligibly small at any T. The results for $\langle S^2\rangle^{1/2}$ thus obtained for $C_{18}E_8$ micelles are summarized in Table 3.

Molar mass M_w dependence of $\langle S^2\rangle_{app}^{1/2}$ is exhibited in Figure 7 for the $C_{18}E_8$ micelles at various T ranging from 30.0 to 50.0 °C. All of the data points form a single composite curve irrespective of temperature and concentration, suggesting that the values of $\langle S^2\rangle_{app}^{1/2}$ determined at finite c correspond to those for the individual micelles free from inter- and intramicellar interactions or excluded volume effects. The solid curve shows the best-fit theoretical values of $\langle S^2\rangle$ calculated for the wormlike chain model by[20]

$$\lambda^2\langle S^2\rangle = \frac{\lambda L}{6} - \frac{1}{4} + \frac{1}{4\lambda L} - \frac{1}{8\lambda^2L^2}(1 - e^{-2\lambda L}) \qquad (14)$$

along with the relation

$$L = \frac{4\upsilon M_w}{\pi N_A d^2} + \frac{d}{3} \qquad (15)$$

In the calculation, the d value 3.2 nm obtained in the preceding section was used, and then the value of λ^{-1} was

TABLE 1: Values of M_w and R_H for $C_{14}E_8$ Micelles at Various T and c

10^2c/g cm^{-3}	$10^{-4}M_w$	R_H/nm[a]	10^2c/g cm^{-3}	$10^{-4}M_w$	R_H/nm[a]
T = 40.0 °C			T = 55.0 °C		
0.8457	5.26	4.90	0.4950	41.5	11.4
0.9095	5.45	3.56	0.8409	54.1	16.4
1.305	6.52	6.27	0.9043	67.3	20.1
1.432	6.82	4.70	1.298	70.5	25.6
2.028	8.13	5.41	1.424	83.9	29.2
2.703	9.42	6.53	2.016	97.1	40.6
3.751	11.4	8.45	2.688	115	59.2
			3.729	182	53.1
T = 45.0 °C			T = 60.0 °C		
0.4669	7.64	4.33	0.4940	71.8	16.8
0.8441	9.93	6.32	0.8393	93.8	22.6
0.9078	10.3	5.50	0.9026	97.3	25.2
1.303	12.3	8.41	1.296	116	33.7
1.429	12.9	6.71	1.421	122	34.5
2.024	15.4	8.15	2.012	146	47.8
2.698	17.8	9.38	2.683	168	66.4
3.744	21.0	11.9	3.723	199	98.9
T = 50.0 °C			T = 65.0 °C		
0.4959	17.8	7.40	0.4931	112	22.7
0.8424	23.2	8.55	0.8377	147	29.9
0.9060	24.0	10.4	0.9010	152	33.7
1.300	28.8	9.98	1.293	182	49.4
1.426	30.1	11.8	1.419	191	48.4
2.020	35.9	14.0	2.009	228	72.1
2.693	41.5	19.2	2.678	263	114
3.736	49.0	24.3	3.716	310	155

[a] The error limits of the figures are ca. ±5%, although those at low temperatures and concentrations are much larger than this as found in the plots in Figure 8a.

TABLE 2: Values of M_w and R_H for $C_{16}E_8$ Micelles at Various T and c

10^2c/g cm^{-3}	$10^{-4}M_w$	R_H/nm[a]	10^2c/g cm^{-3}	$10^{-4}M_w$	R_H/nm[a]
$T = 25.0$ °C			$T = 40.0$ °C		
0.6998	7.79	3.45	0.6957	53.8	16.1
0.8345	8.54	4.53	0.8298	58.7	16.6
0.9718	9.20	5.01	0.9660	63.4	11.4
1.979	13.3	7.96	1.967	90.6	23.3
2.997	16.6	10.1	2.979	112	42.1
$T = 30.0$ °C			$T = 45.0$ °C		
0.6985	8.59	4.40	0.6943	119	23.1
0.8317	9.39	4.94	0.8282	130	27.1
0.9698	10.1	5.25	0.9641	141	25.3
1.975	14.6	8.78	1.963	201	48.8
2.991	18.3	11.1	2.973	248	90.2
$T = 35.0$ °C			$T = 50.0$ °C		
0.6971	9.88	5.12	0.6930	197	34.9
0.8315	10.8	5.20	0.8266	215	40.4
0.9679	11.6	4.47	0.9621	232	40.3
1.971	16.6	7.86	1.959	331	79.0
2.985	20.5	11.8	2.967	409	149

[a] The error limits of the figures are ca. ±5%, although those at low temperatures and concentrations are much larger than this as found in the plots in Figure 8b.

determined as 38.0 nm to achieve the best fit to the observed results. It was found that the calculated results well-explained the observed behavior of $\langle S^2\rangle_{app}^{1/2}$. This agreement again shows that the $C_{18}E_8$ micelles assume a wormlike shape.

Hydrodynamic Radius of the Micelle The apparent hydrodynamic radius $R_{H,app}$ as a function of c has been evaluated from the mutual diffusion coefficient D shown in Figure 3 by[14,26,27]

$$D = \frac{(1 - \nu c)^2 M}{6\pi\eta_0 N_A R_{H,app}}\left(\frac{\partial\pi}{\partial c}\right)_{T,p} \qquad (16)$$

where M is the molar mass of the solute, η_0 is the solvent viscosity, and $(\partial\pi/\partial c)_{T,p}$ is the osmotic compressibility. In this evaluation, we have used the SLS data for $(\partial\pi/\partial c)_{T,p}$ together with the values of $M_w(c)$ obtained in the previous section in place of M. The values of $R_{H,app}$ thus determined at various T are summarized in Tables 1, 2, and 3 for $C_{14}E_8$, $C_{16}E_8$, and $C_{18}E_8$ micelles, respectively, along with the values of M_w. It was found that at any given T, $R_{H,app}$ increases with increasing c, although not shown graphically here. The increase of $R_{H,app}$ may reflect two effects, micellar growth in size and enhancement of the effects of the intermicellar hydrodynamic interactions with increasing c. Thus, the $R_{H,app}$ values do not necessarily correspond to those for isolated micelles.

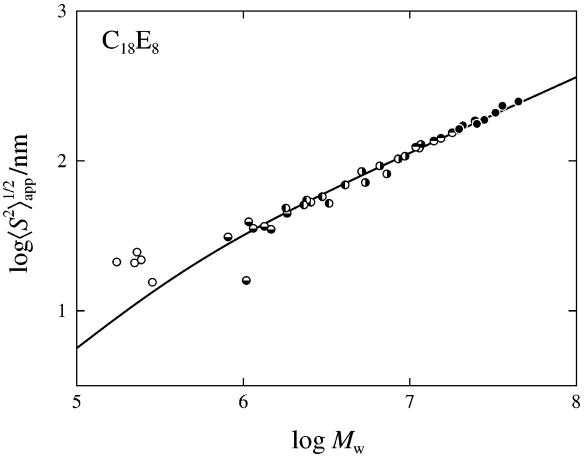

Figure 7. Double-logarithmic plots of $\langle S^2\rangle_{app}^{1/2}$ against M_w. Various symbols have the same meaning as those in Figure 2c. The solid curve represents the theoretical values calculated by eqs 14 and 15.

In Figure 8, parts a−c, $R_{H,app}$ values are double-logarithmically plotted against M_w for $C_{14}E_8$, $C_{16}E_8$, and $C_{18}E_8$ micelles, respectively. As M_w is decreased, i.e., c is lowered, $R_{H,app}$ at each given T decreases following the curve convex downward shown by the dashed line. The data points at different T seem to form asymptotically a single composite curve at small M_w.

TABLE 3: Values of M_w, R_H, and $\langle S^2\rangle^{1/2}$ for $C_{18}E_8$ Micelles at Various T and c

10^2c/g cm^{-3}	$10^{-4}M_w$	R_H/nm[a]	$\langle S^2\rangle^{1/2}$/nm[a]	10^2c/g cm^{-3}	$10^{-4}M_w$	R_H/nm[a]	$\langle S^2\rangle^{1/2}$/nm[a]
$T = 30.0$ °C				$T = 40.0$ °C			
0.1975	17.4		21.1	0.1968	514	36.0	84.9
0.3256	22.2		20.8	0.2175	540	57.2	71.8
0.3500	23.0		24.6	0.3243	659	45.8	92.5
0.3949	24.4	6.03	21.9	0.3934	728	49.8	81.8
0.5402	28.4	9.48	15.5	0.5381	851	81.6	103
0.6507	31.1	9.19		0.6483	935	97.7	107
1.011	38.5	8.77		1.007	1170	180	129
$T = 33.0$ °C				$T = 45.0$ °C			
0.1973	80.9	14.0	31.1	0.1964	1090	56.5	124
0.2180	85.1	23.4		0.2170	1140	89.8	122
0.3252	104	11.9	15.9	0.3237	1400	82.4	135
0.3495	108		39.3	0.3927	1540	102	141
0.3945	115	14.5	35.5	0.5371	1800	163	154
0.5396	134	21.0	36.6	0.6471	1980	214	161
0.6500	147	27.3	34.9	1.005	2470	325	185
1.009	183	29.2	44.7				
$T = 35.0$ °C				$T = 50.0$ °C			
0.1971	180	20.0	48.4	0.1960	1980	84.3	163
0.2179	189	37.3		0.2166	2080	126	172
0.3250	231	22.8	50.9	0.3231	2530	127	177
0.3942	255	27.6	53.0	0.3919	2800	155	187
0.5392	298	37.9	57.5	0.5361	3270	275	209
0.6495	327	47.4	52.0	0.6458	3600		233
1.009	409	58.6	69.0	1.003	4490	578	249

[a] The error limits of the figures are ca. ±5%, although those at low temperatures and concentrations are much larger than this as found in the plots in Figures 7 and 8c.

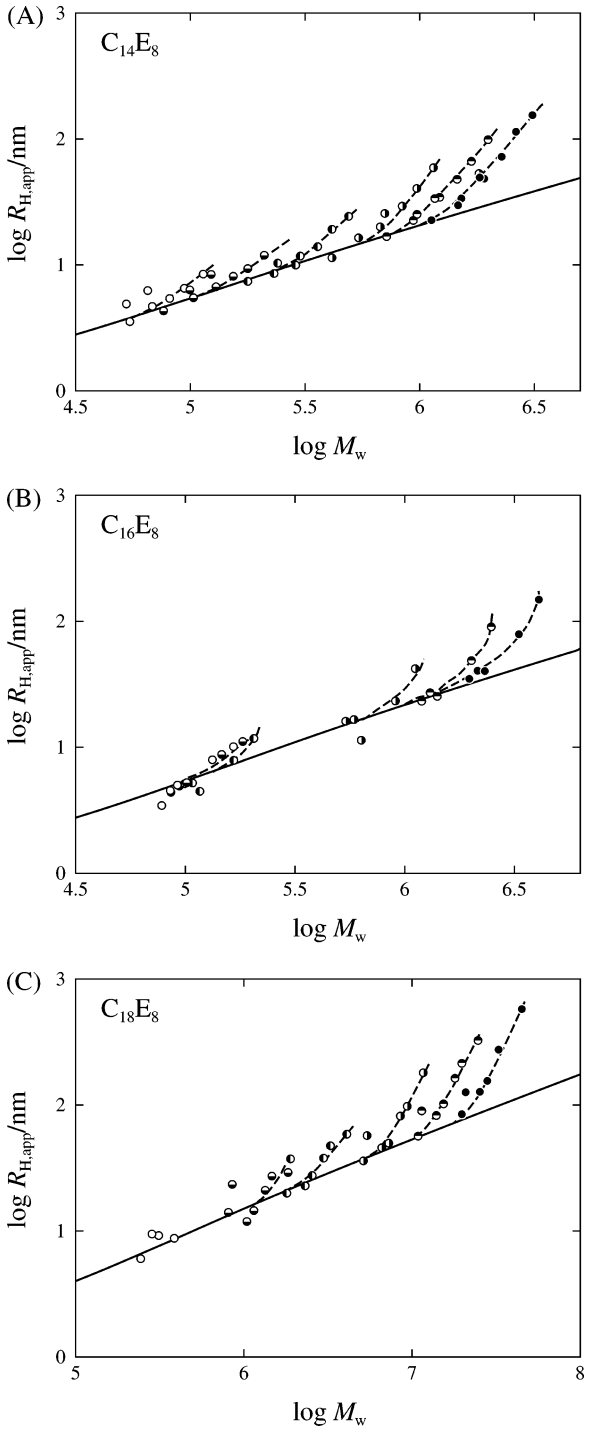

Figure 8. (a) Double-logarithmic plots of $R_{H,app}$ against M_w for all of the $C_{14}E_8$ solutions. Various symbols have the same meaning as those in Figure 3a. The dashed curves are drawn as guidelines. The solid curve represents the theoretical values calculated by eqs 15 and 17. (b) Double-logarithmic plots of $R_{H,app}$ against M_w for all of the $C_{16}E_8$ solutions. Various symbols have the same meaning as those in Figure 3b. The dashed curves are drawn as guidelines. The solid curve represents the theoretical values calculated by eqs 15 and 17. (c) Double-logarithmic plots of $R_{H,app}$ against M_w for all of the $C_{18}E_8$ solutions. Various symbols have the same meaning as those in Figure 3c. The dashed curves are drawn as guidelines. The solid curve represents the theoretical values calculated by eqs 15 and 17.

This result suggests that the effects of the intermicellar hydrodynamic interactions on $R_{H,app}$ become less significant as c is lowered and are negligible in the asymptotic region of low c. Thus, the data points at small M_w at each fixed T may be regarded to give the relationship between R_H and M_w for the isolated micelles. These results are similar to the previous findings for $C_{12}E_6$ and $C_{14}E_6$ micelles.[14]

The translational diffusion coefficient D is formulated, by Norisuye et al.[17] for the wormlike spherocylinder model and by Yamakawa et al.[18,19] for the wormlike cylinder model, as a function of L with including the parameters d and λ^{-1}. From these theories, we may derive the expression for R_H as a function of L, d, and λ^{-1} over the entire range of L including the sphere, i.e., the case $L = d$. It reads

$$R_H = \frac{L}{2f(\lambda L, \lambda d)} \tag{17}$$

The expression for the function f is so lengthy that we refer it to the original papers.[17,18,19] By eqs 15 and 17, the theoretical values of R_H have been calculated as a function of M_w for various values of λ^{-1} with the use of the d values 2.3, 2.4, and 3.2 nm determined above for the $C_{14}E_8$, $C_{16}E_8$, and $C_{18}E_8$ micelles, respectively. In Figure 8, the solid lines are best-fit curves to the data points for which the effects of the intermicellar hydrodynamic interactions are considered to be negligible. It was found that the theoretical curves well-described the observed behavior of R_H as a function of M_w. The curve fittings yield a λ^{-1} value of 18.0 ± 2 nm for the $C_{14}E_8$ micelles, 24.0 ± 2 nm for the $C_{16}E_8$ micelles, and 25.0 ± 2 nm for the $C_{18}E_8$ micelles. The last value for the $C_{18}E_8$ micelles is considerably smaller than the value 38.0 nm obtained above from the analysis of $\langle S^2 \rangle$. This difference may be attributed to the fact that there is a distribution in micellar size and different averages are reflected in $\langle S^2 \rangle_c^{1/2}$ and R_H. It has been theoretically shown[15,25] that micelles with sufficiently large aggregation number N have the most probable distribution and the distribution affords a value ca. 2 as the ratio of the weight-average aggregation number N_w to the number-average N_n irrespective of T and c. It is anticipated that the ratio $N_w/N_n = 2$ is realized at the limit of extensive micellar growth, which can be ascertained by the setup of the relation $M_w \propto c^{1/2}$ as observed in Figure 4 in the present case. Thus, the micelles observed in this study are considered to have the most probable distribution in size, and the distribution affects the evaluation of λ^{-1} from $\langle S^2 \rangle^{1/2}$ and R_H.

The λ^{-1} values indicate that the present micelles are rather stiff compared to typical flexible polymers[28] but far from rigid rod. They increase with increasing alkyl chain length of C_iE_8 molecules, implying that the strength of the hydrophobic interaction among surfactant molecules is a dominant factor of the rigidity of the micelles.

Micelle Structure. The contour length L of the C_iE_8 micelles have been calculated by eq 15 from the values of $M_w(c)$ and d obtained above. Figure 9 shows concentration dependence of log L for each of the micelles at the highest temperature examined in this study. In Figure 10, log L at $c = 0.01$ g/cm^3 is plotted against T. For all the micelles, L becomes larger as c or T is increased. It was found that the micelles grow to a greater length as the alkyl chain length of the surfactant molecules becomes longer. This result may come from the thermodynamic reason that attractive interactions among C_iE_8 molecules become stronger with increasing i as demonstrated above by the values of g_2 (Figure 5).

The spacings s between the hydrophilic tails of adjacent surfactant molecules on the micellar surface are evaluated from the values of d, L, and the aggregation number N calculated from M_w. The s value obtained is ca. 1.46 nm for the $C_{14}E_8$ micelles, ca. 1.46 nm for the $C_{16}E_8$ micelles, and ca. 1.29 nm for the $C_{18}E_8$ micelles irrespective of c and T. The result indicates that the micelles are formed and grow in the way that

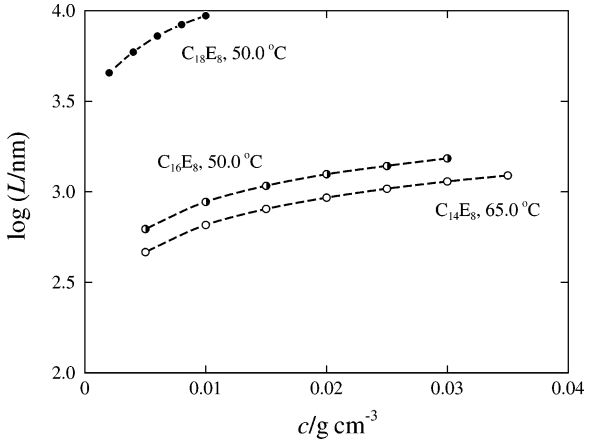

Figure 9. Concentration dependence of L for the $C_{14}E_8$ micelles at 65.0 °C, $C_{16}E_8$ micelles at 50.0 °C, and $C_{18}E_8$ micelles at 50.0 °C.

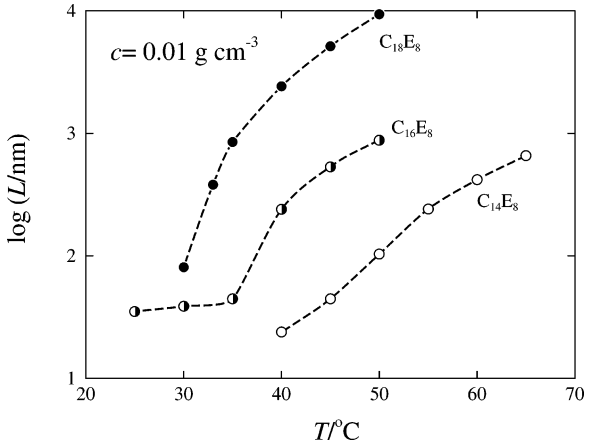

Figure 10. Temperature dependence of L at $c = 0.01$ g/cm^3 for the $C_{14}E_8$ (unfilled circles), $C_{16}E_8$ (half-filled circles), and $C_{18}E_8$ micelles (filled circles).

the hydrophilic groups of the C_iE_8 molecules are located at intervals of these s values on the micellar surface on the average. These s values are not significantly different from one another, presumably reflecting that the hydrophilic groups are the same in the three surfactants. According to the rotational isomeric state (RIS) model calculations by Flory,[29] the root-mean-square end-to-end distance $\langle R^2\rangle^{1/2}$ of octaoxyethylene is 1.33 nm. The present value of the spacings s is comparable to this value. The approximate coincidence may suggest that the octaoxyethylene chain is moving by taking a random orientation in water. The RIS calculation also gives 1.15 nm for $\langle R^2\rangle^{1/2}$ of *n*-tetradecane in $C_{14}E_8$, 1.27 nm for *n*-hexadecane in $C_{16}E_8$, and 1.40 nm for *n*-octadecane in $C_{18}E_8$. The calculations give d values of ca. 3.8, 3.9, and 4.1 nm for the $C_{14}E_8$, $C_{16}E_8$, and $C_{18}E_8$ micelles, respectively, if it is assumed that the alkyl chains of the surfactant molecules exist in the hydrophobic core in a similar state to the bulk state of amorphous polyethylene and that the octaoxyethylene chains are oriented straightforward in a radial direction from the center line of the cylindrical micelle. The calculated d values are rather large compared with the present experimental results. The difference also suggests that the octaoxyethylene chain is oriented at random on the micellar surface.

Conclusion

In the present work, we have determined shape, size, and flexibility of the C_iE_8 micelles with $i = 14$, 16, and 18 at finite surfactant concentrations c from SLS and DLS experiments by employing the same method as used in the previous study for the $C_{12}E_6$ and $C_{14}E_6$ micelles.[14] The results of $Kc/\Delta R_0$ from SLS have been analyzed with the aid of the thermodynamic theory[15] for light scattering of micelle solutions formulated with wormlike spherocylinder model. The analyses have yielded the molar mass $M_w(c)$ as a function of c and the cross-sectional diameter d. The excellent agreement between the calculated and observed $Kc/\Delta R_0$ as a function of c indicates that the C_iE_8 micelles assume the shape of flexible spherocylinders in dilute solutions.

The mean-square radius of gyration $\langle S^2\rangle$ and the hydrodynamic radius R_H of the individual isolated micelles as functions of $M_w \equiv M_w(c)$ have been successfully described by the corresponding to theories for the wormlike chain and the wormlike spherocylinder models, respectively. The values of the stiffness parameter λ^{-1} evaluated from the fitting of the calculated values for $\langle S^2\rangle$ or R_H to the experimental results have revealed that the micelles are far from rigid rods, although considerably stiff compared with typical flexible polymers.

It has been found that the C_iE_8 micelles grow in length to a greater extent for larger i. The finding may imply that attractive interactions among surfactant molecules, by which micelles are formed, are stronger for C_iE_8 molecules with longer hydrophobic chain of alkyl group, as clearly evidenced by the large differences in the free-energy parameter g_2. While the cross-sectional diameter d of the cylindrical micelles becomes larger in the order of the $C_{14}E_8$, $C_{16}E_8$, and $C_{18}E_8$ micelles, the spacings s of the adjacent hydrophilic chains on the micellar surface have been found to have approximately the same values for all the C_iE_8 micelles.

Acknowledgment. The authors are grateful to Professor Takahiro Sato at Osaka University and also to members of the NKO Academy for valuable discussions and comments.

References and Notes

(1) Bernheim-Groswasser, A.; Wachtel, E.; Talmon. Y. *Langmuir* **2000**, *16*, 4131.
(2) Brown, W.; Johnson, R.; Stilbs, P.; Lindman, B. *J. Phys. Chem.* **1983**, *87*, 4548.
(3) Kato, T.; Seimiya, T. *J. Phys. Chem.* **1986**, *90*, 1986.
(4) Brown, W.; Rymdén, R. *J. Phys. Chem.* **1987**, *91*, 3565.
(5) Brown, W.; Pu, Z.; Rymdén, R. *J. Phys. Chem.* **1988**, *92*, 6086.
(6) Imae, T. *J. Phys. Chem.* **1988**, *92*, 5721.
(7) Richtering, W.; Burchard, W.; Finkelmann, H. *J. Phys. Chem.* **1988**, *92*, 6032.
(8) Kato, T.; Anzai, S.; Seimiya, T. *J. Phys. Chem.* **1990**, *94*, 7255.
(9) Strunk, H.; Lang, P.; Findenegg, G. H. *J. Phys. Chem.* **1994**, *98*, 11557.
(10) Schurtenberger, P.; Cavaco, C.; Tiberg, F.; Regev, O. *Langmuir* **1996**, *12*, 2894.
(11) Jerke, G.; Pedersen, J. S.; Egelhaaf, S. U.; Schurtenberger, P. *Langmuir* **1998**, *14*, 6013.
(12) Glatter, O.; Fritz, G.; Lindner, H.; Brunner-Papela, J.; Mittelbach, R.; Strey, R.; Egelhaaf, S. U. *Langmuir* **2000**, *16*, 8692.
(13) Carale, T. R.; Blankschtein, D. *J. Phys. Chem.* **1992**, *96*, 455.
(14) Yoshimura, S. Shirai, S. Einaga, Y. *J. Phys. Chem. B.* **2004**, *108*, 15477.
(15) Sato, T. *Langmuir* **2004**, *20*, 1095.
(16) Koyama, R.; Sato, T. *Macromolecules* **2002**, *35*, 2235.
(17) Norisuye, T.; Motowoka, M.; Fujita, H. *Macromolecules* **1979**, *12*, 320.
(18) Yamakawa, H.; Fujii, M. *Macromolecules* **1973**, *6*, 407.
(19) Yamakawa, H.; Yoshizaki, T. *Macromolecules* **1979**, *12*, 32.
(20) Benoit, H.; Doty, P. *J. Phys. Chem.* **1953**, *57*, 958.
(21) Pike, E. R.; Pomeroy, R. M.; Vaughan, J. M. *J. Chem. Phys.* **1975**, *62*, 3188.
(22) Einaga, Y.; Mitani, T.; Hashizume, J.; Fujita, H. *Polym. J.* **1979**, *11*, 565.
(23) Blankschtein, D.; Thurston, G. M.; Benedek, G. B. *J. Chem. Phys.* **1986**, *85*, 7268.

(24) Cates, M. E.; Candou, S, J. *J. Phys.: Condens. Matter* **1990**, *2*, 6869.
(25) Zoeller, N.; Lue. L.; Blankschtein, D. *Langmuir* **1997**, *13*, 5258.
(26) Berne, B.; Pecora, R. *Dynamic Light Scattering*; Wiley: New York, 1976.
(27) Stepánek, P.; Brown, W.; Hvidt, S. *Macromolecules* **1996**, *29*, 8888.
(28) Tamai, Y.; Konishi, T.; Einaga, Y.; Fujii, M.; Yamakawa, H. *Macromolecules* **1990**, *23*, 4067.
(29) Flory, P. J. *Statistical Mechanics of Chain Molecules*; John Wiley & Sons: New York; 1969.